

Correlations between Hurst Exponent and maximal Lyapunov Exponent for some low-dimensional discrete conservative dynamical systems

Mariusz Tarnopolski

Received: date / Accepted: date

Abstract The Chirikov standard map and the 2D Froeschlé map are investigated. The Hurst Exponent (HE) and maximal Lyapunov Exponent (mLE) plots in a mixed parameter-initial condition space are calculated for a few thousand values. It is found that for both maps the HE distribution follows extremely well the mLE distribution in this space. The correlations are 0.95 and 0.88 for the Chirikov and 2D Froeschlé maps, respectively. Despite the statistical distributions differ significantly between the maps, they have common properties, hence a universal relation is speculated to underly this correlation. As the numerical calculation of the HE is more time-consuming, a machine learning procedure is performed and the HE distributions are reproduced based on several values of the mLE. A perfect agreement is found, which allows to investigate statistical properties of HE distributions based on easier to compute mLE values.

Keywords Conservative Systems · Maximal Lyapunov Exponent · Hurst Exponent · Machine Learning

PACS 05.45.Ac · 05.45.Pq · 05.45.Tp · 05.40.Fb

1 Introduction

Dynamical systems play a crucial role in the description of physical reality, being applied in fields such as cosmology [30], astrophysics [35, 21], nuclear physics [17], environmental science [31], financial analysis [9], among others. Nonlinear systems can exhibit chaotic behaviour [3, 23], e.g. Chirikov standard map [6] being a discrete volume preserving 2D example or Lorenz [14] and Hénon-Heiles [12] systems, being 3D dissipative and 4D conservative continuous systems, respectively. Continuously, new chaotic systems are being discovered [4, 34]. Conservative systems, being Hamiltonian [5, 15], exhibit a complicated mixture of chaotic and regular

Mariusz Tarnopolski
Astronomical Observatory, Jagiellonian University
Cracow, Poland
E-mail: mariusz.tarnopolski@uj.edu.pl

components in phase space and do not possess a strange attractor [10]. Hence, a wide range of maximal Lyapunov Exponent (mLE) is expected to be found in such systems. Moreover, a mixed parameter–initial condition space allows to properly trace the route to chaos via period doubling [19]. On the other hand, a question about inferring chaotic dynamics from a single-variable time series was raised and efficiently answered decades ago [33, 27, 11].

Time series may be described by their statistical properties. One of its descriptors is a Hurst Exponent (HE) [13, 20], which is a measure of persistency or long-range memory [16] that is widely used, e.g., in financial analyses [2] and Solar physics [29]. HEs proved to be useful indicators of morphological type in astrophysical processes [18]. Despite being intrinsically unpredictable, classical chaotic time series stem from deterministic processes, therefore order is expected to underly their dynamics (e.g. strange attractors or fractal basins of attraction [24, 32]). A common behaviour is occurrence of irregular *switchings* from temporarily regular oscillations to apparently chaotic variations. This leads to an observation that chaotic time series should yield an HE greater than 0.5 (persistent behaviour), and indeed it was reported in [29] that a chaotic solution of Lorenz system possesses an HE=0.87.

In this paper, correlations between mLEs and HEs are investigated for 2D conservative maps and machine learning is performed to reproduce statistical HE distribution given an mLE distribution, as the computation of HE is more time-consuming than the mLE value.

2 Methods

Consider two common conservative 2D systems: the Chirikov standard map

$$\begin{cases} p_{n+1} = p_n + \frac{K}{2\pi} \sin(2\pi x_n) & \text{mod } 1, \\ x_{n+1} = x_n + p_{n+1} & \text{mod } 1, \end{cases} \quad (1)$$

and the 2D Froeschlé map¹ [8]

$$\begin{cases} p_{n+1} = p_n - k \sin(x_n + p_n) & \text{mod } 2\pi, \\ x_{n+1} = x_n + p_n & \text{mod } 2\pi, \end{cases} \quad (2)$$

both symplectic and governed by a single nonlinear parameter and exhibiting, besides strictly regular and chaotic, also sticky behaviour. The modulus keeps the variables confined to a square box and this condition is released for the rest of the paper, treating the evolution of both systems as a 2D unbounded (deterministic) walk. This is necessary for mLE calculation and makes the HE computation less ambiguous in the sense that it allows the HE estimation algorithm to fully capture (anti-)persistency of time series. The mLEs are calculated via eigenvalues of Jacobian matrices. Equations (1) and (2) are iterated 10^4 times, and for HE computation the first 4000 values are discarded to be sure transient behaviour, e.g. stickiness, is skipped over, and p_n is used for both maps as x_n is monotonic, hence yielding HE=1.

¹ Lacking an entrenched name, to differentiate from its well-studied 4-dimensional version, this map is herein termed as the *2D Froeschlé map* as it first appeared in [8].

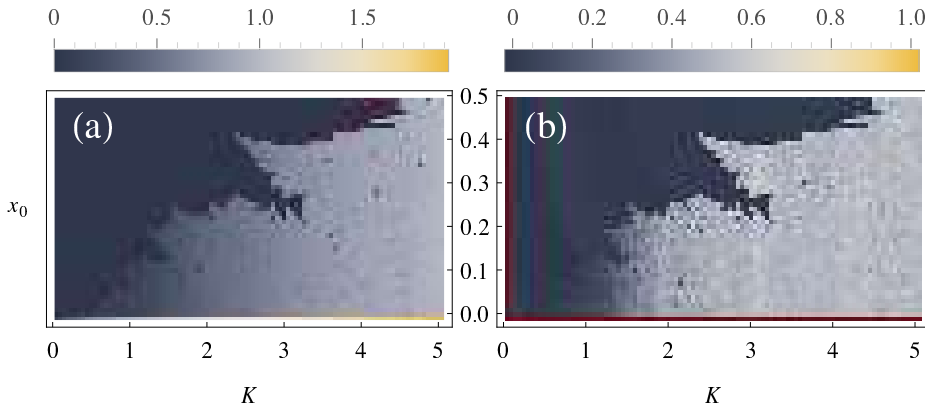


Fig. 1 (colour online) (a) mLEs and (b) HEs in the mixed space $K \times x_0$ with $p_0 = 0.0$ for Chirikov standard map, 10^4 iterations and a grid of $101 \times 51 = 5151$ points. Red points mark indeterminate values. Note different colour scales used.

Among many existing computational algorithms for HE estimation (Rescaled Range [20], Detrended Fluctuation Analysis [25, 26], wavelet approach [28], to mention only a few), Detrended Moving Average (DMA) [1] is exceptional as it does not divide a whole dataset into subsamples and is therefore used herein.

A MATHEMATICA[®] v10.0.2 computer algebra system is used throughout this paper.

3 Results

3.1 Chirikov standard map

A map of mLEs in a mixed space $K \times x_0$ with $p_0 = 0.0$ is shown in Fig. 1(a) (some of the mLEs were undetermined). This is a recalculation of Fig. 2 in [19] but due to symmetry only non-negative x_0 's are taken into account. Although the overall picture sketched by both Figures is consistent with each other, note slight differences in mLE values, that are caused by applying different algorithms: in [19] an mLE was extracted from a timeseries as described in [33] (Manchein, personal communication). The difference is especially striking for the unstable line $x_0 = 0.0$, for which mLEs obtained via algorithm [33] are about two times smaller than the ones from this paper's approach. On the other hand, regular domain in Fig. 1(a) seems to possess no structure, contrary to Fig. 2 in [19]: this is simply caused by a narrow interval of mLEs in this region and a colour scale applied; this was verified by plotting only mLEs corresponding to regular motion. As this work is not focused on detailed aspects of the mixed space, already discussed in [19], but rather on general features, this is not a concern.

Next, a similar plot for HEs was drawn and is displayed in Fig. 1(b). The unstable line $x_0 = 0.0$ had to be discarded as the HEs were undetermined by the algorithm. An automatic fitting of a straight line on a log-log plot of each $\sigma_k \propto k^{\text{HE}}$ relation was performed to extract HEs [1]. Histograms in Fig. 2 (mLE, HE, standard deviation, range of the 99% confidence interval and Pearson's R^2 of

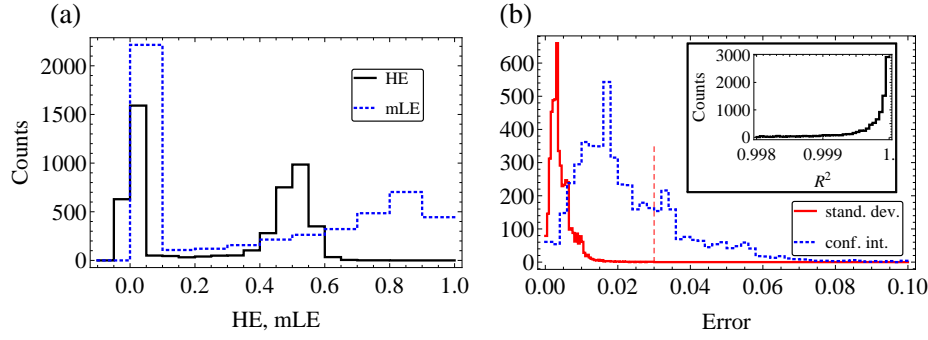


Fig. 2 (colour online) (a) Distributions of HEs and mLEs. Two distinct peaks are related to regular and chaotic domain of the mixed space. The mLE values greater than 1.0 are not displayed as they account for only 1.6% of all values. (b) HE errors; solid red – standard deviation, std, of the fitted slope, dashed blue – width of the 99% confidence interval, α . Maximal value of std is 0.03 (marked with a vertical red line), while α is not greater than 0.164. Inset shows the Pearson coefficient R^2 ; displayed bins contain 94% of counts. The minimal R^2 is 0.9732.

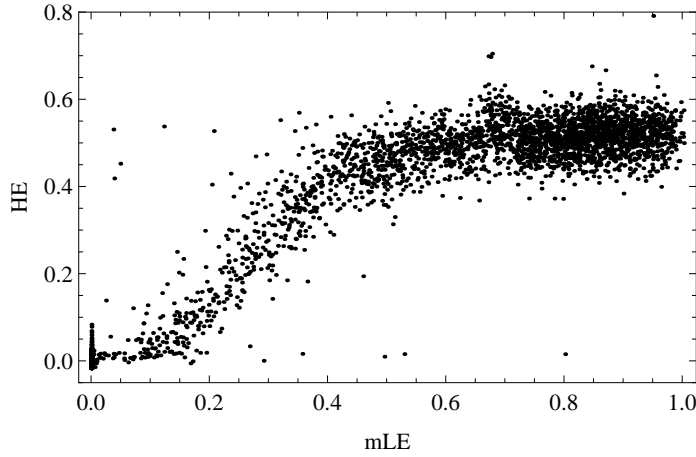


Fig. 3 Scatter plot for mLE–HE relation; 4962 points are displayed for which $r_p = 0.95$ and $r_s = 0.83$.

each HE estimate) convince that the fitting procedure returned reliable estimates of HE values. Interestingly, the HEs follow in general a wave-like structure of the regular region. A higher resolution figure (i.e., consisting of a finer grid) might possibly reveal a complex structure of these waves, however this is outside the scope of this work.

After dropping indeterminate outcomes, 4962 points with numerical values were left for which a scatter plot is shown in Fig. 3. A Pearson correlation $r_p = 0.95$, Spearman rank $r_s = 0.83$, and p -values for both are numerically equal to zero.

Despite a negligible amount of outliers, the correlation between mLEs and HEs is very high, and as the computation of HEs took 18 times longer than of mLEs,

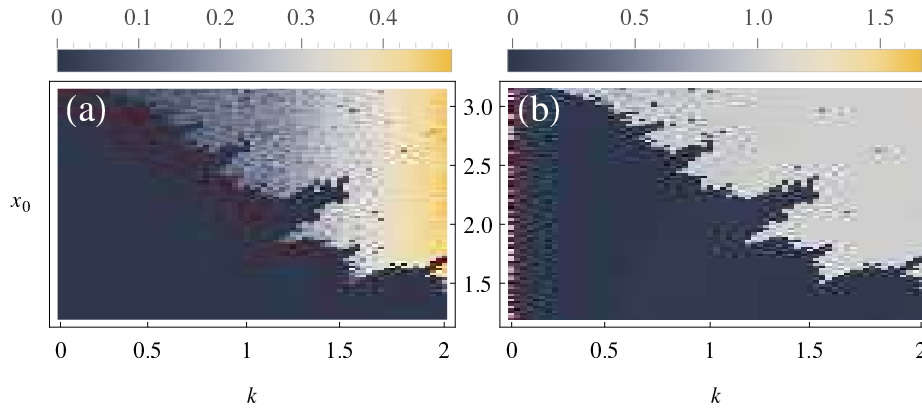


Fig. 4 (colour online) (a) mLEs and (b) HEs in the mixed space $k \times x_0$ with $p_0 = 0.0$ for a 2D Froeschlé map, 10^4 iterations and a grid of $67 \times 98 = 6566$ points. Red points mark indeterminate values. Note different colour scales used.

this relation will provide insight into statistical distribution of HEs based on mLEs only.

3.2 2D Froeschlé map

Next, the map (2) is investigated in the same manner as in the previous subsection. Figures 4(a) and (b) show the mLE and HE distributions, respectively, in the mixed space $k \times x_0$ with $p_0 = 0.0$ and exhibit the same structure as the Chirikov standard map does, i.e. bifurcating tongues of regular motion creeping in the chaotic zone. A significant difference is that the HEs gather around two extreme values, i.e. 0.0 for regular and 1.0 for chaotic regions, different from the Chirikov standard map and with no gradient in between. Note a negligible amount of high HEs along the line $k = 0.0$ in Fig. 4(b).

Statistical distributions, displayed in Fig. 5(a) (note a logarithmic scale for the ordinate), reveal an almost uniform distribution of mLEs for chaotic motion. Fittings performed for HE computation are not as reliable as in the former case, though. For example, the Pearson coefficient R^2 can attain a value as small as 0.0. On the other hand, a majority of fittings are characterized by errors small enough to allow examining at least general features of the HE distribution (compare with Fig. 5(b)). Although the maximal 99% confidence interval range can be as wide as the whole theoretical range of HE values (spanning a unit interval from 0 to 1), the standard deviations do not exceed the value of 0.19, and *i*) are centered around small absolute values, as indicated by the histogram in Fig. 5(b), and *ii*) allow to distinguish chaotic from regular motions due to clearly separated peaks near extremal values of HEs.

Thus, as the scatter plot in Fig. 6 for this map does not possess as unambiguous structure as for the previous one, the distributions in Fig. 5 assure that the relation between mLEs and HEs is correctly grasped, at least as a first approximation. Note that the flat cut-off from above in Fig. 6 is a true feature and is not an artifact due to dropping indeterminate values (as $0 \leq \text{HE} \leq 1$). Moreover, the higher the

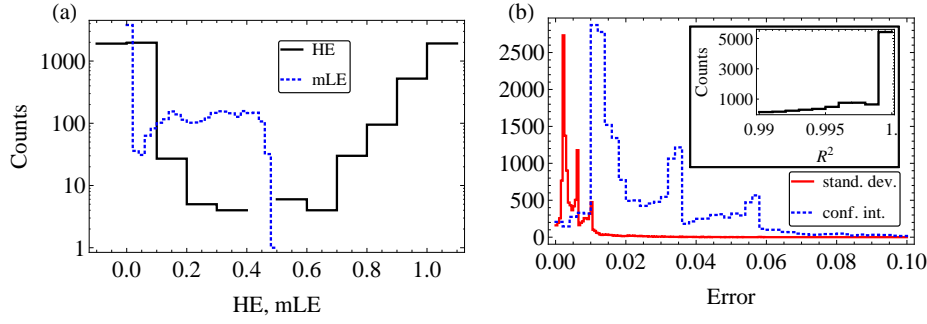


Fig. 5 (colour online) (a) Distributions of HE and mLE. Two distinct HE peaks are related to regular and chaotic domain of the mixed space. The mLE values are not greater than 0.5 and have an approximately uniform distribution inside the chaotic region. (b) HE errors; solid red – standard deviation, std, of the fitted slope, dashed blue – width of the 99% confidence interval, α . Maximal value of std is 0.19, while α spans an interval from 0 to 1.04. Inset shows the Pearson coefficient R^2 ; displayed bins contain 84% of counts. The minimal R^2 is 0. Extreme values of α and R^2 are rare enough to be treated as outliers.

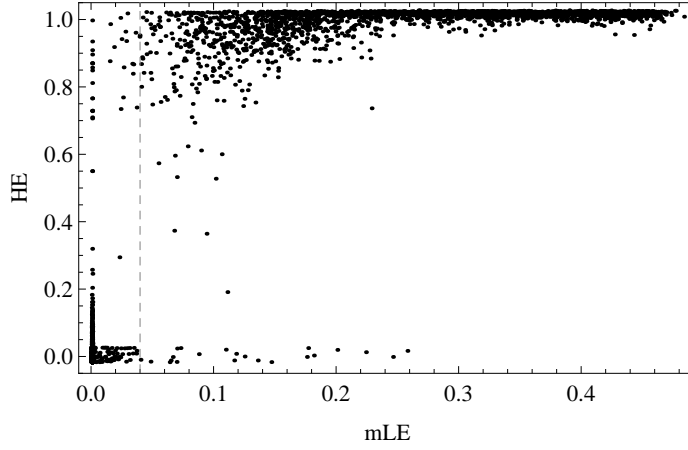


Fig. 6 Scatter plot for mLE–HE relation; 6314 points are displayed for which $r_p = 0.89$, $r_s = 0.75$, and p -values numerically equal to zero.

mLE, the smaller the scatter among corresponding HE values, and the critical mLE value equal to 0.04 (vertical dashed line in Fig. 6) separates accurately small HEs from larger ones, or equivalently in this case, values corresponding to regular and chaotic zones in the mixed space.

4 Machine learning

Using built-in functionalities of MATHEMATICA[®], machine learning is performed on mLE–HE relations from Section 3. A `NearestNeighbors` method is employed and training on a set $\{(param, x_0, mLE)_i \rightarrow HE_i\}_{i=1}^N$ is performed, where N is an appropriate number of points used with respect to the map under consideration,

and *param* is a nonlinear parameter, K or k in Eq. (1) and (2), respectively. The output are machine-learnt functions $p(x)$. Next, $\approx 2.0 \cdot 10^5$ mLEs are produced for the Chirikov standard map on a grid of 1001×201 points in the mixed space, and similarly $\approx 2.4 \cdot 10^5$ mLEs on a grid of 501×486 points for the 2D Froeschlé map. Resultant mLE distributions are shown in Fig. 7(a) and (b) and are consistent with Fig. 2(a) and Fig. 5(a). For the Chirikov standard map two distinct peaks are easily distinguishable, while the distribution for the 2D Froeschlé map is nearly flat for non-zero mLEs and with a steep decrease just before 0.5. Functions $p(x)$ were then applied and the reproduced HE distributions are displayed in Fig. 7(c) and (d). To emphasize that the underlying initial mLE distribution is crucial and $p(x)$ itself is not informative, HE distributions are computed also for artificial, flat mLE ones. This resulted in a uniformly mapped, via $p(x)$, HE distributions, significantly different from the real ones, especially for the Chirikov standard map. The difference for 2D Froeschlé map is visible in the height of the peak near zero-values, as the rest of the real distribution is almost flat, hence not really different from the artificial one.

These machine-learnt HE distributions were eventually mapped on the mixed space and the results are shown in Fig. 7(e) and (f). Regular and chaotic regions are sharply divided, as in Fig. 1 and Fig. 4, and the coverage is nearly perfect. Note that, e.g. for the Chirikov standard map, $p(x)$ is obtained only based on mLEs and HEs *both* determinate, i.e., as described in Section 3, extreme mLEs along the unstable line $x_0 = 0.0$ were discarded. This is why the absolute colour functions in Fig. 1(b) and Fig. 7(e) are different, yet the relative distributions almost identical. The same applies for the 2D Froeschlé map in Fig. 4(b) and Fig. 7(f).

Despite the mLE–HE relations in Fig. 3 and Fig. 6 are significantly different, their overall behaviour is similar, i.e. after an initial rise the relations plateau. To highlight similarities rather than differences, another machine learning is performed, this time using a `NeuralNetwork` method in order to produce smooth curves, displayed in Fig. 8. Note that both relations were normalized on the axis for comparative purposes.

The relations have a common plateau at approximately half of the largest attainable mLE and a steep increase before. For the Chirikov standard map there is an inflection point at 0.26, while the relation for the 2D Froeschlé map is characterized by two slopes before the plateau. Left part of the curves is obviously influenced by the amount of nearly-zero mLEs, which is approximately linearly dependent on the size of the regular zone relative to the chaotic region. This means that $p(x)$ may be different if the mixed space is bounded differently. Nevertheless, as the mLE and HE distributions in the chaotic zones are not entirely characterized by a single peak, the inferred $p(x)$ is likely to describe the mLE–HE relations correctly. There is a possibility that both curves belong to the same family.

5 Conclusions

To conclude, a high correlation between mLEs and HEs was found for two 2D conservative maps. Machine learning was performed in order to obtain HE distributions based on faster to compute mLE distributions, which gave nearly perfect results compared to training sets. Machine-learnt HE distributions in a mixed space reproduce extremely well the ones from the training sets. Another machine

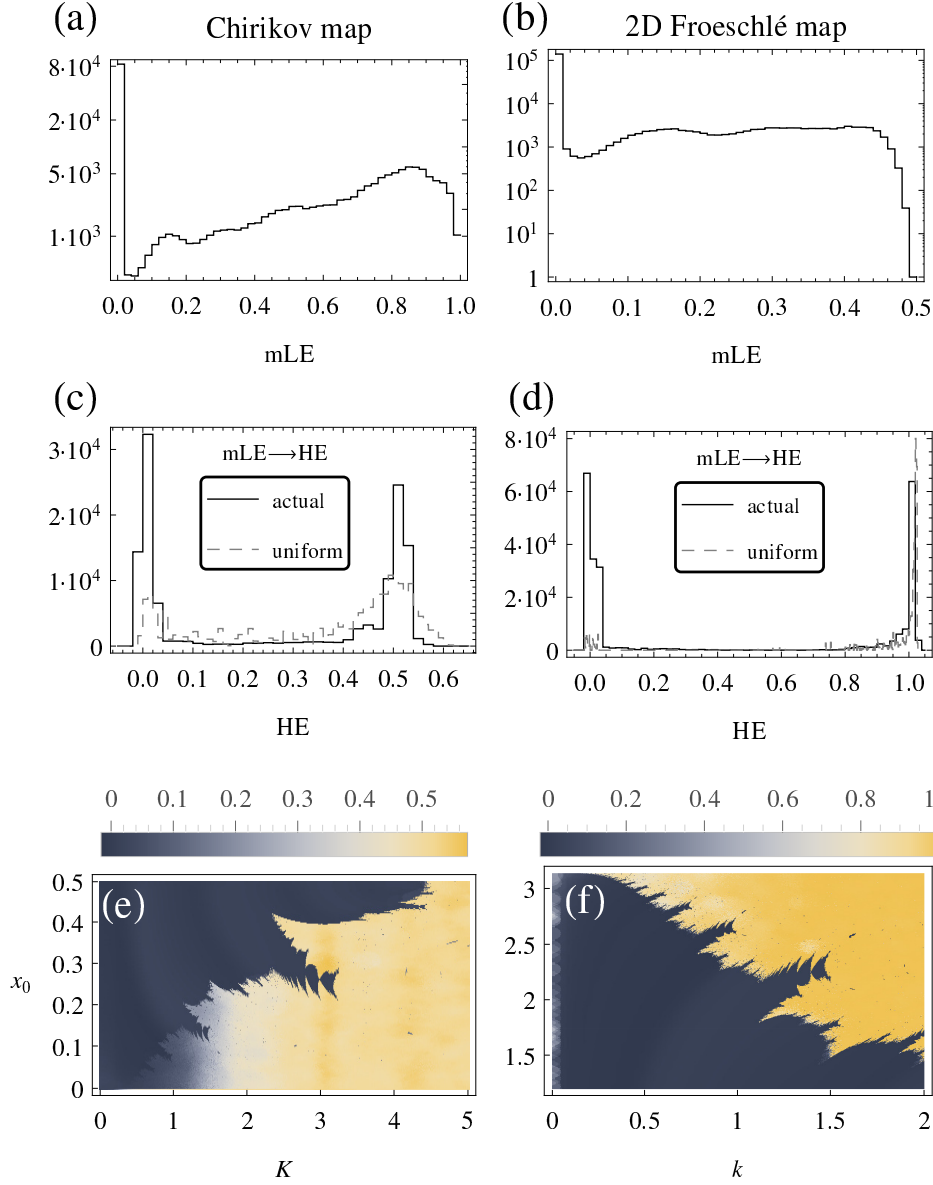


Fig. 7 (colour online) *Left column:* Chirikov standard map. *Right column:* 2D Froeschlé map. (a)—(b) Actual mLE distributions for $\approx 2.0 \cdot 10^5$ and $2.4 \cdot 10^5$ values, respectively. (c)—(d) HE distributions obtained by the machine-learned function $p(x)$ with a `NearestNeighbors` method; solid black – actual distributions obtained by applying $p(x)$ to (a) and (b); dashed gray – comparison distributions obtained by applying $p(x)$ to artificial uniform distributions (at the level of ≈ 5000). (e)—(f) HE distributions in the mixed space obtained by applying $p(x)$ to (a) and (b). Note different colour scales used.

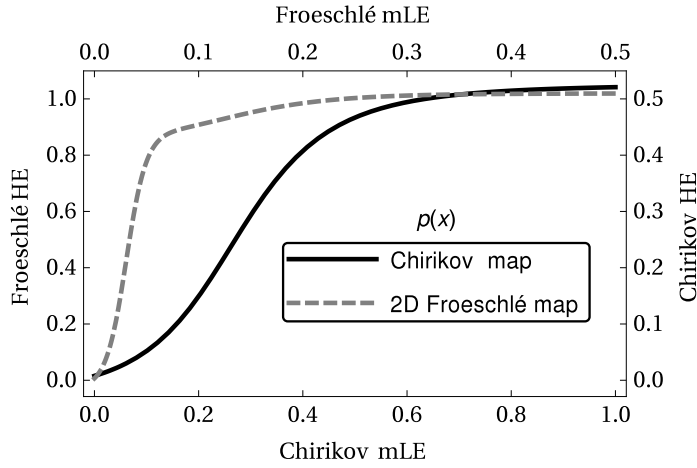


Fig. 8 Machine learnt $p(x)$ for the Chirikov standard map (black solid) and 2D Froeschlé map (dashed gray) obtained with a `NeuralNetwork` method applied to the training sets; this produces a smooth curve that allows to investigate the overall behaviour of the mLE–HE relation. Note different axis for the two maps and that $p(x)$ is not the same as previously used as here it is obtained with a different method.

learning method revealed similarities among mLE–HE relations that allow to formulate a question about universality of the dependence found. A hypothesis that these relations belong to the same family is put forward. On the other hand, the maps under consideration are closely related, hence the similarity in mLE and HE distributions, to some extent, might be expected. However, the strength of this similarity and a cause underlying it as well as visible differences, remains an open issue. This hypothesis does not seem so unlikely when one notes that a conservative Hénon map is related to the Chirikov standard map [22]. Its verification will require investigating other maps and detailed theoretical work. A first step should be differentiating between symplectic and non-symplectic conservative mappings. A natural question about mLE–HE correlations in dissipative systems remains open, and eventually leads to examining continuous, Hamiltonian and dissipative, dynamical systems.

The results presented here may be a step towards verifying presence of chaos in economics [7] by means of a reversed mapping, $\text{HE} \rightarrow \text{mLE}$ [2], however this would require a reliable model to build a training set on.

References

1. Alessio, E., Carbone, A., Castelli, G., Frappietro, V.: Second-order moving average and scaling of stochastic time series. *Eur. Phys. J. B* **27**(2), 197–200 (2002)
2. Carbone, A., Castelli, G., Stanley, H. E.: Time-dependent Hurst exponent in financial time series. *Physica A* **344**(1–2), 267–271 (2004)
3. Alligood, K. T., Sauer, T. D., Yorke, J. A.: *Chaos: an Introduction to Dynamical Systems*, Springer New York (2000)
4. Alpar, O.: Analysis of a new simple one dimensional chaotic map. *Nonlinear Dyn.* **78**(2), 771–778 (2014)
5. Bountis, T., Skokos, H.: *Complex Hamiltonian Dynamics*, Springer Berlin Heidelberg (2012)

6. Chirikov, B. V.: A universal instability of many-dimensional oscillator systems. *Phys. Rep.* **52**(5), 263–379 (1979)
7. Faggini, M.: Chaotic time series analysis in economics: Balance and perspectives. *Chaos* **24**(4), 042101 (2014)
8. Froeschlé, C.: On the number of isolating integrals in systems with three degrees of freedom. *Astrophys. Space Sci.* **14**(1), 110–117 (1971)
9. Gao, Q., Ma, J.: Chaos and Hopf bifurcation of a finance system. *Nonlinear Dyn.* **58**(1–2), 209–216 (2009)
10. Greiner, W.: *Classical Mechanics. Systems of Particles and Hamiltonian Dynamics*. Springer Berlin Heidelberg (2010)
11. Hegger, R., Kantz, H., Schreiber, T.: Practical implementation of nonlinear time series methods: The TISEAN package. *Chaos* **9**(2), 413–435 (1999)
12. Hénon, M., Heiles, C.: The applicability of the third integral of motion: some numerical experiments. *Astron. J.* **69**(1), 73–79 (1964)
13. Hurst, H. E.: Long-term storage capacity of reservoirs. *Trans. Am. Soc. Civ. Eng.* **116**, 770–799 (1951)
14. Lorenz, E. N.: Deterministic Nonperiodic Flow, *J. Atmos. Sci.* **20**(2), 130–141 (1963)
15. Lowenstein, J. H.: *Essentials of Hamiltonian Dynamics*, Cambridge University Press (2012)
16. Machado, J. A. T., Lopes, A. M.: The Persistence of Memory. *Nonlinear Dyn.* (2014) doi:10.1007/s11071-014-1645-1
17. MacKay, R. S., Meiss, J. D. (Eds.): *Hamiltonian Dynamical Systems: A Reprint Selection*. CRC Press (1987)
18. MacLachlan, G. A., Shenoy, A., Sonbas, E., Coyne, R., Dhuga, K. S., Eskandarian, A., Maximon, L. C., Parke, W. C.: *Mont. Not. R. Astron. Soc.* **436**(4), 2907–2914 (2013)
19. Manchein, C., Beims, M. W.: Conservative Generalized Bifurcation Diagrams. *Phys. Lett. A* **377**(10–11), 789–793 (2013)
20. Mandelbrot, B. B., Wallis, J. R.: Noah, Joseph, and Operational Hydrology. *Water Resour. Res.* **4**(5), 909–918 (1969)
21. Manos, T., Machado, R. E. G.: Chaos and dynamical trends in barred galaxies: bridging the gap between N -body simulations and time-dependent analytical models. *Mont. Not. R. Astron. Soc.* **438**(3), 2201–2217 (2014)
22. Miguel, N., Simó, C., Vieiro, A.: From the Hénon Conservative Map to the Chirikov Standard Map for Large Parameter Values. *Regular and Chaotic Dynamics* **18**(5), 469–489 (2013)
23. Ott, E.: *Chaos in Dynamical Systems*, Cambridge University Press (2002)
24. Ott, E.: Basin of attraction. *Scholarpedia* **1**(8):1701 www.scholarpedia.org/article/Basin_of_attraction. Accessed 12 January 2015
25. Peng, C.-K., Buldyrev, S. V., Havlin, S., Simons, M., Stanley, H. E., Goldberger A. L.: Mosaic organization of DNA nucleotides. *Phys. Rev. E* **49**(2), 1685–1698 (1994)
26. Peng, C.-K., Havlin, S., Stanley, H., Goldberger, A. L.: Quantification of scaling exponents and crossover phenomena in nonstationary heartbeat time series. *Chaos* **5**(1), 82–87 (1995)
27. Rosenstein, M. T., Collins, J. J., De Luca, C. J.: A practical method for calculating largest Lyapunov exponents from small data sets. *Physica D*, **65**(1–2), 117–134 (1993)
28. Simonsen, I., Hansen, A., Nes O. M.: Determination of the Hurst exponent by use of wavelet transforms. *Phys. Rev. E* **58**(3), 2779–2787 (1998)
29. Suyal, V., Prasad, A., Singh H. P.: Nonlinear Time Series Analysis of Sunspot Data. *Sol. Phys.* **260**(2), 441–449 (2009)
30. Wainwright, J., Ellis, G. F. R.: *Dynamical Systems in Cosmology*. Cambridge University Press (1997)
31. Wang, R., Xiao, D.: Bifurcations and chaotic dynamics in a 4-dimensional competitive Lotka-Volterra system. *Nonlinear Dyn.* **59**(3) 411–422 (2010)
32. Weisstein, E. W.: Newton’s Method. *MathWorld—A Wolfram Web Resource*. <http://mathworld.wolfram.com/NewtonsMethod.html>. Accessed 12 January 2015
33. Wolf, A., Swift, J. B., Swinney H. L., Vastano J. A.: Determining Lyapunov Exponents from a Time Series. *Phys. D* **16**(3), 285–317 (1985)
34. Zhang, X., Zhu, H., Yao, H.: Analysis of a new three-dimensional chaotic system. *Nonlinear Dyn.* **67**(1), 335–443 (2012)
35. Zotos, E. E., Caranicolas, N. D.: Order and chaos in a new 3D dynamical model describing motion in non-axially symmetric galaxies. *Nonlinear Dyn.* **74**(4), 1203–1221 (2013)